PHYSICAL REVIEW B **86**, 064417 (2012)

Magnetic coupling between Sm^{3+} and the canted spin in an antiferromagnetic $SmFeO_3$ single crystal

L. G. Marshall,[1] J.-G. Cheng,[1] J.-S. Zhou,[1,*] J. B. Goodenough,[1] J.-Q. Yan,[2,3] and D. G. Mandrus[2,3]
[1]*Materials Science and Engineering Program/Mechanical Engineering, The University of Texas at Austin, Austin, Texas 78712, USA*
[2]*Materials Science and Technology Division, Oak Ridge National Laboratory, Oak Ridge, Tennessee 37831, USA*
[3]*Department of Materials and Engineering, The University of Tennessee, Knoxville, Tennessee 37996, USA*

(Received 11 May 2012; revised manuscript received 18 July 2012; published 13 August 2012)

The perovskite $SmFeO_3$ exhibits type-*G* antiferromagnetic ordering at $T_N \approx 670$ K and an easy axis rotation transition at $T_{SR} \approx 480$ K. Owing to the peculiar site anisotropy of rare-earth Sm^{3+}, the moment on Sm^{3+} is oriented antiparallel to the canted spin from the Fe^+ sublattice along the *a* axis at $T < T_{SR}$. The development of the magnetic moment on Sm^{3+} as temperature decreases makes it possible to balance the two magnetic moments at T_{comp}. The application of a moderate external magnetic field along the *a* axis can trigger an abrupt reversal of the moment on Sm^{3+} and the canted spin relative to the external field at a temperature around T_{comp}. We report here a study of the field-induced magnetic-moment reversal in a single crystal $SmFeO_3$ by measuring the magnetization and specific heat with the external field along different crystallographic axes.

DOI: 10.1103/PhysRevB.86.064417 PACS number(s): 75.30.Cr, 75.50.Gg, 71.70.Gm

Although the physical properties of the perovskite oxides RMO_3 ($R =$ rare earth, $M =$ transition metal) are dominated by the *M*-ion array, the interaction between the rare-earth *R* and *M* sublattices can induce unusual phenomena such as spin rotation transitions on both sublattices and charge transfers. For example, the sharp metal-insulator transition in the $Pr_{0.5}Ca_{0.5}CoO_3$ perovskite, which was previously attributed to a spin-state transition of Co ions,[1] was recently clarified as being due to a real charge transfer between Pr and Co ions (i.e., $0.5\ Pr^{3+} + Co^{3.5+} \rightarrow 0.5\ Pr^{4+} + Co^{3+}$).[2,3] Recent studies on the perovskite $SmMnO_3$ (Refs. 4 and 5) have shown another unusual magnetic phenomenon associated with the coupling between the rare-earth Sm^{3+} and the Mn^{3+}. In this compound, the Mn^{3+}-ion sublattice exhibits type-*A* antiferromagnetic order below $T_N \approx 60$ K with a weak canted-spin ferromagnetic moment along the crystallographic *c* axis of the *Pbnm* structure. Below T_N, the magnetic moment on Sm^{3+} ions is progressively oriented antiparallel to the canted-spin ferromagnet moment parallel to the *c* axis from the Mn^{3+}-ion array due to an internal exchange field H_{in} along the *c* direction. When a small magnetic field (e.g., 500 Oe) is applied along the *c* axis, the Sm^{3+} moment dominates the canted-spin Mn^{3+} moment below a compensation temperature $T_{comp} \approx 9$ K, leading to a negative magnetization. Moreover, applying an external magnetic field $H_{ex} \geqslant 1$ T along the *c* axis results in a simultaneous reversal of both the moment on Sm^{3+} and the canted spin moment from Mn^{3+} relative to the direction of the external field at temperatures $T_t^{\pm} = T_{comp} \pm \delta$; this reversal is manifest as a sudden jump in the magnetic susceptibility, specific heat, and dielectric constant.[4] The thermal hysteresis loop $\Delta T = T_t^{+} - T_t^{-}$ associated with this first-order transition depends sensitively on the magnitude of H_{ex} (i.e., the larger H_{ex}, the smaller ΔT). This unusual magnetic moment reversal is due to the peculiar site anisotropy on Sm^{3+} that places the rare-earth moment antiparallel to the exchange field from the Mn^{3+} array. This type of temperature-induced magnetization reversal has also been observed in some other RMO_3 antiferromagnetic materials.[6–10] In comparison, the moment on Nd^{3+} in the perovskite $NdMnO_3$ is along the direction of the canted-spin from Mn^{3+} (Refs. 11 and 12); while the moment on Pr^{3+} is perpendicular to the canted spin on Mn^{3+} in the perovskite $PrMnO_3$ (Ref. 12). To verify whether all the observations made on the $RMnO_3$ crystals are applicable only to the type-*A* antiferromagnetic (AF) magnets or are universal for all types of AF magnets with a canted spin structure, we have carried out a similar study on a perovskite $SmFeO_3$ crystal. In this compound, the Fe^{3+} sublattice exhibits a type-*G* antiferromagnetic order at a $T_N \approx 670$ K (Ref. 13). In contrast to $SmMnO_3$, the spin direction on Fe^{3+} in $SmFeO_3$ changes from the *b* axis at $T < T_N$ to the *c* axis at $T < T_{SR} = 480$ K (Ref. 14), which makes the canted moment along the *a* axis at $T < T_{SR}$. It is also reported that the magnetization M_a for the magnetic field ($H = 0.01$ T) along the *a* axis crosses zero at $T \approx 5$ K (Refs. 14 and 15), which may signal a magnetic moment compensation between the moments on Sm^{3+} and the canted spin on Fe^{3+} similar to that between the moment on Sm^{3+} and the canted spin on Mn^{3+} in $SmMnO_3$. Therefore, we have explored the possible moment reversal at higher magnetic fields. In this paper, we report measurements of the magnetization and specific heat on a single crystal of $SmFeO_3$ under different magnetic fields applied along all principal crystallographic axes. Nearly identical observations made on $SmFeO_3$ and on $SmMnO_3$ give rise to a simple rule that the moments on Sm^{3+} are always opposite to the canted-spin moment of the MO_3 array in the orthorhombic perovskites.

The $SmFeO_3$ single crystal used in the present study was grown in an infrared-heating image furnace (NEC SC-M35HD). The starting ceramic rods of $SmFeO_3$ were the product of a reaction between Sm_2O_3 (Alfa Aesar, 99.9%) and Fe_2O_3 (Alfa Aesar, 99.998%) in a 1:1 ratio. The crystals were grown by the floating zone method[16] in a flow of air. The phase purity was confirmed by powder x-ray diffraction. Laue back reflection was used to check the crystal quality and to orient the crystals along the three principal axes with an error less than 1°. Measurements of the magnetization have been carried out in a commercial superconducting quantum interference device (SQUID) magnetometer (Quantum Design). The specific heat was measured in different applied magnetic fields with a Physical Property Measurement System (Quantum Design) by using the two-τ relaxation method at temperatures from 2 to 20 K and under different magnetic fields up to 10 T. The background from the sample holder and the Apiezon N grease

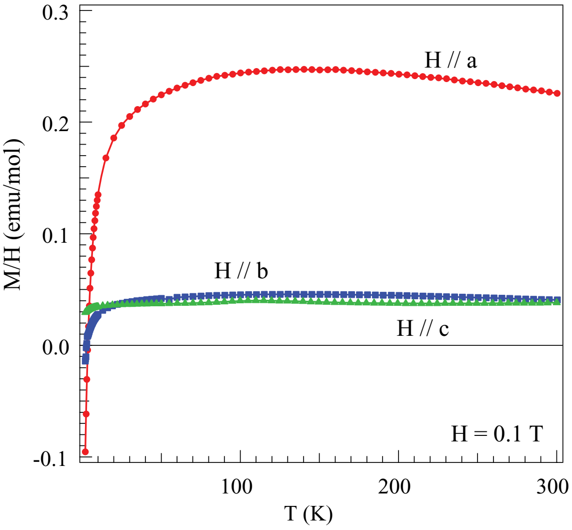

FIG. 1. (Color online) Temperature dependence of the magnetization $M(T)$ of the $SmFeO_3$ single crystal with magnetic field $H = 0.1$ T applied along all three major crystallographic axes a, b, and c. The crystal weights for the magnetization measurements are as follows: 11.9 mg (a axis oriented), 7.3 mg (b axis oriented), 70.3 mg (c axis oriented).

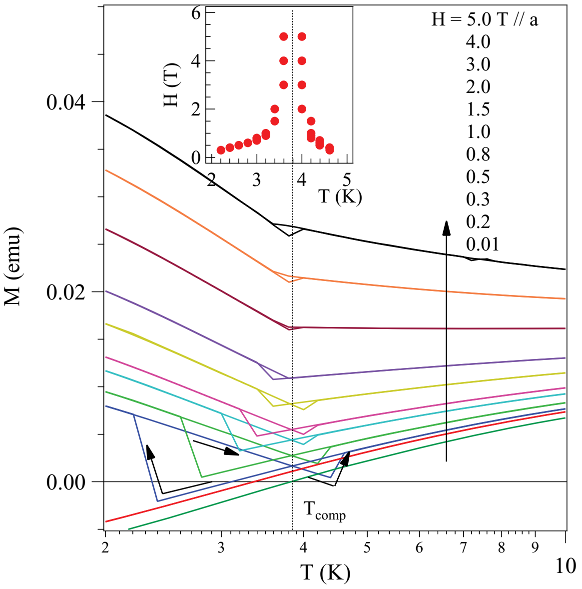

FIG. 2. (Color online) Temperature dependence of magnetization $M(T)$ for the $SmFeO_3$ crystal with magnetic field applied along the a axis; the inset plot shows the transition temperatures T_t and T_t' found for different magnetic fields.

was recorded in different magnetic fields and was subtracted from the total specific heat.

Figure 1 shows the temperature dependence of the magnetization $M(T)/H$ of the $SmFeO_3$ crystal oriented along the three principal axes with $H = 0.1$ T and in the temperature range 2–300 K, which is far below the long-range antiferromagentic ordering temperature $T_N \approx 670$ K and the spin-reorientation temperature $T_{SR} = 480$ K. Consistent with the fact that the magnetic easy axis of $SmFeO_3$ changes from the b axis to the c axis and the canting direction is along the a axis below T_{SR}, the $M_a(T)$ is nearly one order of magnitude higher than $M_b(T)$ and $M_c(T)$. The main features of the $M(T)$ curves occur at low temperatures where the moment on Sm^{3+} starts to align with the exchange field from the Fe^{3+} sublattice. The influence of Sm^{3+} moments on the overall magnetization along the a axis shows up at $T \approx 140$ K. The net moment experiences a crossover from a dominant canted spin from the Fe^{3+} sublattice to a dominant Sm^{3+} moment on cooling through $T_{comp} = 3.7$ K. The observed M_a in our crystal grown with the floating-zone method is almost identical to that measured by Lee *et al.*;[14] their crystal was grown with the flux method. We noticed that the $M_b(T)$ curve in Fig. 1 also crosses zero at $T \approx 3.7$ K and resembles the same feature as that of $\chi_a(T)$. The most likely reason for this behavior is the twinning formed during crystal growth. As a matter of fact, twinning on the *ab* plane has been widely observed in the orthorhombic *Pbnm* perovskite oxides in which there is a phase transition to the phase with higher symmetry (i.e., the rhombohedral phase *R*-3*c* or the tetragonal phase *I*4/*mcm* at high temperatures). The twinning is difficult to detect with Laue back reflection, especially in the case of $a \approx b$. However, this kind of twinning should not affect the magnetization along the c axis and this is indeed confirmed by the $M_c(T)$ shown in Fig. 1. A totally detwinned $SmFeO_3$ crystal requires a slow cooling process under uniaxial pressure through the *Pbnm*-to-*R3*-*c* phase transition. This phase transition temperature remains unknown to us. The crystals used in this study are not totally detwinned. In the following, we will focus on measurements of the $SmFeO_3$ crystal with magnetic field oriented along the a axis where the highest magnetization has been detected.

The $M_a(T)$ curves of the $SmFeO_3$ crystal shown in Fig. 2 were measured with thermal cycling between 2 and 10 K under various magnetic fields H_{ex} up to 5 T. At $H_{ex} > 0.2$ T, an abrupt change of $M_a(T)$ has been observed on cooling at $T_t = T_{comp} - \delta$ and warming at $T_t' = T_{comp} + \delta'$, resulting in an asymmetric butterfly-shaped hysteresis loop. The field dependence of T_t and T_t' are shown in the inset of Fig. 2. With increasing H_{ex}, the thermal hysteresis loop $\Delta T = T_t - T_t'$ becomes smaller and the loop becomes less obvious at $H_{ex} > 1.5$ T. The magnetization M no longer crosses zero for $H_{ex} > 0.3$ T. These features observed for M_a in the present $SmFeO_3$ are very similar to those of the M_c found in a $SmMnO_3$ crystal with H_{ex} applied along the c axis.[4] From these observations and their comparison with those for $SmMnO_3$, we conclude that applying an external field $H_{ex} > 0.2$ T along the spin canting direction leads to a simultaneous flipping of both the Sm^{3+} moments and the canted-spin magnetization of the FeO_3 array.

As demonstrated in the case of a $SmMnO_3$ single crystal,[4] the magnetic-field-induced moment reversal can be verified by low-temperature specific-heat measurements. The ground state of the free Sm^{3+} ion, $^6H_{5/2}$, is split into three Kramer's doublets in the crystal field. According to the result of inelastic neutron scattering on isostructural $SmNiO_3$, these three doublets are separated by 220 and 450 K, respectively.[17] The internal exchange field on the Sm^{3+} site further splits the lowest Kramer's doublet by $\Delta E = \Delta_g/k_B$, where k_B is the Boltzmann constant. This splitting is reflected in the specific heat $C(T)$ measurement by a Schottky anomaly at $T < 20$ K. Figure 3

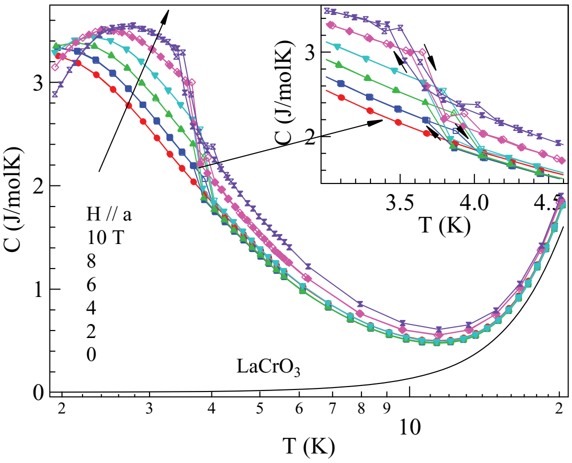

FIG. 3. (Color online) Temperature dependence of specific heat $C(T)$ for the SmFeO$_3$ crystal with different magnetic fields applied along the a axis; the insert shows the $C(T)$ near T_t. Solid symbols: $C(T)$ measured on cooling down; open symbols: $C(T)$ measured on heating up. A thermal hysteresis loop near T_t becomes visible at $H \geqslant 2$ T. The $C(T)$ of LaCrO$_3$ is shown for comparison. The disk-shaped crystal for the specific heat measurement was oriented with Laue back reflection in such a way that the a axis (and therefore the direction of external magnetic field) is normal to the crystal surface. However, the curve fitting to the magnetic field dependence of the gap Δ in Fig. 5 indicates that the external magnetic field is actually applied inside the ab plane and closer to the b axis. This is due to twinning effects in the crystal, as described in the main text. The crystal weight is 8.1 mg.

shows the specific heat $C(T)$ of a SmFeO$_3$ crystal measured upon both heating and cooling in the temperature range 2–20 K and under various magnetic fields up to 10 T applied along the a axis. The $C(T)$ at $H = 0$ exhibits a dramatic increase down to 2 K relative to that of LaCrO$_3$ due to the Schottky contribution of Sm^{3+}; but a complete profile of the Schottky contribution to $C(T)$ is not fully developed at 2K, the lowest temperature in this study since the gap $\Delta_g/k_B(H = 0)$ is small. There is no observable difference between the curves during heating up and cooling down. Although the spin reversal can be clearly seen in the magnetization measurement of Fig. 1 with H_{ex} as large as 1 T, the magnetic field is still too small to make an obvious change on the Schottky anomaly to $C(T)$, which is dominated by a huge internal exchange field $H_{in} \sim 11$ T as determined by the following curve fitting. With increasing applied magnetic field, the Schottky anomaly moves to higher temperatures, which allows us to see the more complete profile of $C(T)$ from the Schottky anomaly. Moreover, in accordance with the abrupt change at T_t in the $M_a(T)$ data, an abrupt drop or jump of $C(T)$ was observed at T_t and T_t' during heating or cooling, which can be seen more clearly in the inset of Fig. 3. However, these anomalies are less pronounced than those observed in SmMnO$_3$ (Ref. 4).

Fitting the $C(T)$ under different magnetic fields to the formula of the Schottky anomaly, we can obtain the quantitative information on such parameters as the gap $\Delta_g/k_B(H)$, the internal exchange field H_{in}, the effective moment of the Sm^{3+} ions, as well as the relative orientation of H_{in} with respect to the H_{ex}. We have fitted the $C(T)$ data of SmFeO$_3$ in Fig. 3 by taking into account three contributions (e.g., the lattice and spin wave $C_{lat} + C_{sw}$, the Schottky contribution C_{Sch}, and the crystal-field contribution C_{CF}). Both the $C_{lat} + C_{sw}$ and C_{CF} terms do not contribute to the low-temperature enhancement of $C(T)$. The $C(T)$ of isostructural LaCrO$_3$ was used to represent the $C_{lat} + C_{sw}$, while the crystal-field splitting of Sm^{3+} in SmNiO$_3$ was used to obtain the C_{CF} (Ref. 17), see Ref. 4 for details on how to decompose contributions from C_{lat}, C_{sw}, and C_{CF}. The Schottky contribution C_{Sch} is expressed as

$$C_{Sch} = R(\Delta_g/k_BT)^2 \exp(\Delta_g/k_BT)/[1 + \exp(\Delta_g/k_BT)]^2, \tag{1}$$

where Δ_g/k_B is the splitting of the ground Kramer's doublet, k_B is the Boltzmann constant, and R is the ideal gas constant. For $H_{ex} > 0.3$ T, the external field triggers the moment reversal. In this case, the canting angle and therefore the exchange field at Sm^{3+} varies depending on whether the canted spin direction is parallel or antiparallel to the external field. The canting direction becomes antiparallel to the H_{ex} at $T < T_t$ and parallel at $T > T_t$ as illustrated in Fig. 4. The canting

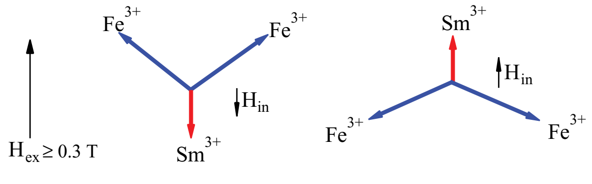

(a) T > T$_t$ (b) T < T$_t$

FIG. 4. (Color online) A schematic view of the relative orientation of the Sm^{3+} moment (H_{in}), the canted-spin ferromagnetic Fe^{3+} moment (// a axis) and the external magnetic field H_{ex} at $T < T_t$ and $T > T_t$.

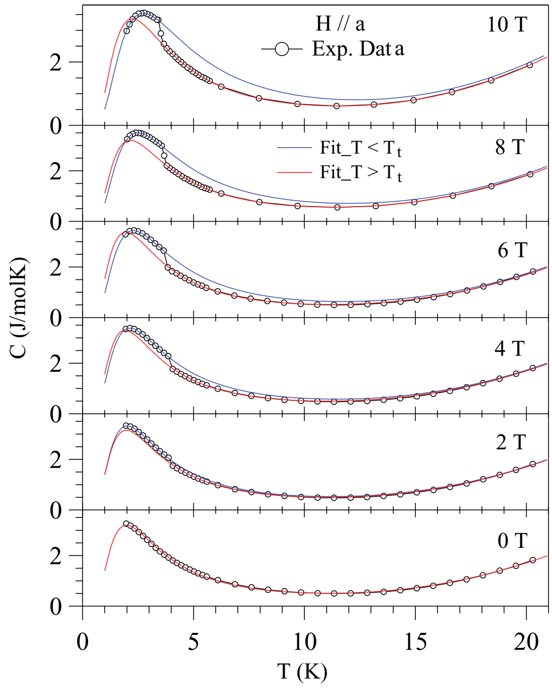

FIG. 5. (Color online) The detailed fitting curves for the $C(T)$ for the SmFeO$_3$ crystal under different magnetic fields.

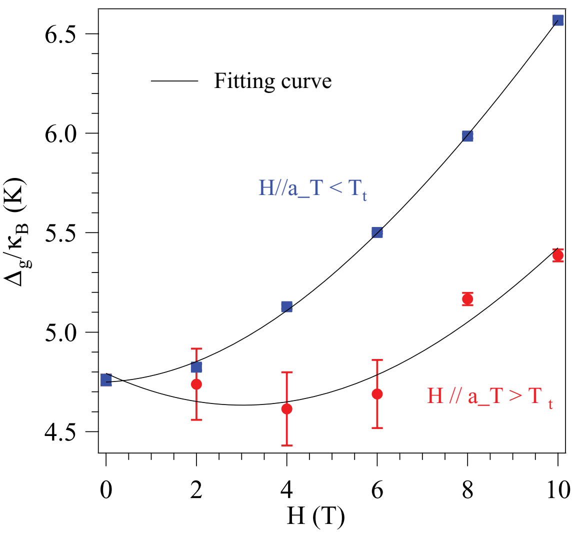

FIG. 6. (Color online) The magnetic field dependence of the energy gap Δ_g/κ_B and the curve fitting by using Eqs. (1) and (2) in the text.

angle and therefore the exchange field at the Sm^{3+} site depends on the configuration between the canted spin and the external magnetic field. The abrupt change of $C(T)$ on crossing T_t truly reflects a discontinuous change of the gap in the Schottky formula. Therefore, we have carried out the fitting procedure separately for $T < T_t$ and $T > T_t$ with two different energy gaps Δ_g/k_B. As shown in Fig. 5, the fitting curves for each field can excellently reproduce the experimental data.

The obtained Δ_g/k_B as a function of external magnetic field H_{ex} is plotted in Fig. 6. As can be seen from the plot, Δ_g/k_B for $T < T_t$ increases gradually with H_{ex}, but it does not follow a linear field dependence of $\Delta_g/k_B \propto H_{in} + H_{ex}$ for $T < T_t$ as expected for the H_{ex} applied along the *a* axis. Similarly, for $T > T_t$, Δ_g/k_B should be proportional to $H_{in} - H_{ex}$. However, we have found that Δ_g/k_B decreases slightly and then increases with H_{ex} with a broad minimum. Although we have applied the external magnetic field H_{ex} along the *a* axis of a crystal disk, the non-linear field dependence of Δ_g/k_B indicates that the H_{ex} is actually neither parallel nor perpendicular to the internal exchange field H_{in}. Taking into account the twin formation within the *ab* plane as already observed in the χ_b, the actual situation in our $C(T)$ measurements could be a combination of the magnetic field effect on both *a* and *b* axes. For a twined crystal, a magnetic field H_{ex} is applied within the *ab* plane and it has an angle θ relative to the *a* axis, the Δ_g/k_B will have the following field dependence:

$$\Delta_g/k_B = 2\mu_{\rm eff}[(H_{\rm ex}\cdot\cos\theta + H_{\rm in})^2 + (H_{\rm ex}\cdot\sin\theta)^2]^{1/2} \quad \text{for} \quad T < T_t, \tag{2}$$

TABLE I. The fitting parameters to $\Delta_g/k_B(H)$ in Fig. 6.

	$T < T_t$	$T > T_t$
$\mu_{\rm eff}/Sm^{3+}$ (μ_B)	0.33 ± 0.01	0.30 ± 0.04
$H_{\rm ex}$ (T)	10.7 ± 0.2	11.8 ± 1.4
θ (°)	88.6 ± 1.3	75.1 ± 4.6

and

$$\Delta_g/k_B = 2\mu_{\rm eff}[(H_{\rm ex}\cdot\cos\theta + H_{\rm in})^2 + (H_{\rm ex}\cdot\sin\theta)^2]^{1/2} \quad \text{for} \quad T > T_t. \tag{3}$$

As shown in Fig. 6, the $\Delta_g/k_B(H)$ for both $T < T_t$ and $T > T_t$ can be described perfectly with Eqs. (2) and (3). The fitting parameters are given in Table I. As can be seen, the parameters at $T < T_t$ and $T > T_t$ are highly consistent with each other, which confirms our assumption and analysis above. The obtained effective moment of Sm^{3+}, 0.33(1) μ_B, is perfectly in line with 0.36 μ_B found in $SmMnO_3$; the $H_{in} \sim 11$ T is smaller than that of ~18 T found in $SmMnO_3$. The angle θ indicates that most of the crystal has its *a* axis perpendicular to the external field in this measurement. The crystal cut for the magnetization measurement with the H_{ex} along the *a* axis has a smaller cross section in the *bc* plane than that used for the specific-heat measurement. Therefore, the chance to include twining domains with different orientations is significantly higher in the crystal for the specific-heat measurement. From the analysis of the specific-heat data, we further confirm the magnetic-field-induced spin reversal of both the Sm^{3+} and the canted-spin ferromagnetic Fe^{3+} moments in $SmFeO_3$.

In conclusion, detailed magnetic measurements and specific-heat analysis on a $SmFeO_3$ single crystal are consistent with the scenario that the rare-earth Sm^{3+} moment is antiparallel to the canted-spin ferromagnetic moment of the Fe^{3+}-ion array along the *a* axis. A moderate external magnetic field $H_{ex} > 0.2$ T applied along the *a* axis can induce a simultaneous reversal of Sm^{3+} and the Fe^{3+} canted-spin moments relative to the external field; the magnetic moment reversal results in a sharp anomaly in both magnetization and specific heat at T_t. The analysis of the $\Delta_g/k_B(H)$ splitting on the Sm^{3+} ions further supports the above scenario. The nearly identical observations in both $SmMnO_3$ and $SmFeO_3$ indicate that the moment reversal should be a generic feature of the Sm^{3+} moment in canted-spin antiferromagentic perovskite oxides.

The work at Austin was supported by NSF (DMR 0904282, DMR 1122603) and the Robert A. Welch foundation (Grant No. F-1066). The work at ORNL was supported by the Division of Materials Sciences and Engineering, Office of Basic Energy Sciences, US Department of Energy.

---

[*] jszhou@mail.utexas.edu

[1] S. Tsubouchi, T. Kyomen, M. Itoh, P. Ganguly, M. Oguni, Y. Shimojo, Y. Mori, and Y. Ishii, Phys. Rev. B **66**, 052418 (2002).

[2] J. Hejtmanek, E. Santava, K. Knizek, M. Marysko, Z. Firak, T. Naito, H. Sasaki, and H. Fujishiro, Phys. Rev. B **82**, 165107 (2010).

[3] J. L. Garcia-Munoz, C. Frontera, A. J. Baron-Gonzalez, S. Valencia, J. Blasco, R. Feyerherm, E. Dudzik, R. Abrudan, and F. Radu, Phys. Rev. B **84**, 045104 (2011).

[4] J.-G. Cheng, J.-S. Zhou, J. B. Goodenough, Y. T. Su, Y. Sui, and Y. Ren, Phys. Rev. B **84**, 104415 (2011).

[5] J.-S. Jung, A. Iyama, H. Nakamura, M. Mizumaki, N. Kawamura, Y. Wakabayashi, and T. Kimura, Phys. Rev. B **82**, 212403 (2010).

[6] J. B. Goodenough and H. C. Nguyen, Acad. Sci. Paris C. R. **319**, 1285 (1994).

[7] J. Mao, Y. Sui, X. Zhang, Y. Su, X. Wang, Z. Liu, Y. Wang, Z. Liu, Y. Wang, R. Zhu, Y. Wang, W. Liu, and J. Tang, Appl. Phys. Lett. **98**, 192510 (2011).

[8] H. C. Nguyen and J. B. Goodenough, Phys. Rev. B **52**, 324 (1995).

[9] K. Yoshii and A. Nakamura, J. Solid State Chem. **155**, 447 (2000).

[10] Y. Ma, M. Guilloux-Viry, P. Barahona, O. Pena, and C. Moure, Appl. Phys. Lett. **86**, 062506 (2005).

[11] A. Munoz, J. A. Alonso, M. J. Martinez-Lope, J. L. Garcia-Munoz, and M. T. Fernandez-Diaz, J. Phys.: Condens. Matter. **12**, 1361 (2000).

[12] J. Hemberger, M. Brando, R. Wehn, V. Yu. Ivanov, A. A. Mukhin, A. M. Balbashov, and A. Loidl, Phys. Rev. B **69**, 064418 (2004).

[13] E. N. Maslen, V. A. Streltsov, and N. Ishizawa, Acta Crystallogr. Sect. B **52**, 406 (1996).

[14] J.-H. Lee, Y. K. Jeong, J. H. Park, M. A. Oak, H. M. Jang, J. Y. Son, and J. F. Scott, Phys. Rev. Lett. **107**, 117201 (2011).

[15] Y. K. Jeong, J.-H. Lee, S.-J. Ahn, and H. M. Jang, Solid State Communications **152**, 1112 (2012).

[16] A. Revcolevschi and R. Collongues, C.R. Seances Acad. Sci., Ser. A **266**, 1797 (1969); A. Revcolevschi, Rev. Int. Htes. Temps. **7**, 73 (1970).

[17] S. Rosenkranz, M. Medarde, F. Fauth, J. Mesot, M. Zolliker, A. Furrer, U. Staub, P. Lacorre, R. Osborn, R. S. Eccleston, and V. Trounov, Phys. Rev. B **60**, 14857 (1999).